AAS 24-305

CISLUNAR TRAJECTORY DESIGN FOR CONSTELLATIONS LEVERAGING SIDEREAL-SYNODIC RESONANT BEHAVIOR

Maaninee Gupta* **and Kathleen C. Howell†**

To establish a comprehensive SSA architecture in cislunar space, space-based sensors that can traverse the expansive volume are currently an option being evaluated. With the availability of unique vantage points across the domain of cislunar space via sidereal resonant orbits, orbits that are additionally commensurate with the lunar synodic period provide options for feasible visibility conditions that persist over time. Metrics for modeling cislunar targets and evaluating their visibility are leveraged to assess and design trajectories for optical observers.

INTRODUCTION

There is an increasing general interest in trajectories within the cislunar regime in support of a wide ranging types of activities, including Space Domain Awareness (SDA) and Space Situational Awareness (SSA) operations. The expanse of cislunar space, that extends beyond the GEO (geosynchronous) belt and towards the lunar orbit, necessitates trajectories that are able to span this vast volume while maintaining access with the Earth.[1] Specifically for supporting SSA needs, i.e., those that entail the foundational, current, and predictive knowledge and characterization of space objects and the space domain, it is likely necessary to design trajectories that can host space-based sensors.[2] As such, orbits constructed in multi-body dynamical models that exhibit repeating geometries under natural dynamical motion offer clear advantages. One option for such orbits include trajectories in sidereal resonance with the Moon, since they naturally remain phased with the lunar orbit while also traversing various different regions within cislunar space. In the Earth-Moon Circular Restricted Three-Body Problem (CR3BP), these orbits exist in families that offer orbits possessing sidereal resonant geometries at different energy levels. From such orbit families, it is also possible to identify orbits that, in addition to providing the unique vantage points exhibited by sidereal resonant orbits, are resonant with the lunar synodic period. This characteristic allows the convenient assessment of visibility conditions in cislunar space, since repeatability relative to the orientation of the Sun is achieved. This investigation provides an overview of such orbits, computed in the Earth-Moon CR3BP, and their application towards the design of space-based optical observer trajectories. Targets that locally and globally describe the volume defined by the cislunar realm are modeled, and the visibility of the various targets is evaluated via the proposed observer trajectories. All the analyses presented in this work are conducted in the Earth-Moon CR3BP to obtain a realistic assessment of the cislunar dynamical environment.

*Ph.D. Candidate, School of Aeronautics and Astronautics, Purdue University, West Lafayette, IN 47907; gupta208@purdue.edu; currently, Postdoctoral Researcher, Texas A&M University, College Station, TX 77843; maanineegupta@tamu.edu

†Hsu Lo Distinguished Professor of Aeronautics and Astronautics, School of Aeronautics and Astronautics, Purdue University, West Lafayette, IN 47907; howell@purdue.edu

BACKGROUND

To model the gravitational environment of cislunar space with reasonable accuracy, a dynamical model that incorporates the influence of both the Earth and the lunar gravity on the motion of a spacecraft is necessary. As such, the Earth-Moon Circular Restricted Three-Body Problem (CR3BP) is employed in the current work for preliminary analysis. A subset of periodic orbits that are constructed in this dynamical model, termed resonant orbits, are introduced for further exploration towards the design of space-based observer trajectories.

Dynamical Model: Circular Restricted Three-Body Problem

The Circular Restricted Three-Body Problem (CR3BP) is an autonomous dynamical model that incorporates the gravitational influences of two planetary bodies, for example, a planet-moon or a Sun-planet pair. In this investigation, the Earth-Moon CR3BP is leveraged for the preliminary assessment of cislunar trajectories. The Earth and the Moon, termed the primaries and denoted as P_1 and P_2, respectively, are assumed to be point masses orbiting their mutual barycenter in circular orbits. The third body models the spacecraft, denoted P_3, that is assumed to be of infinitesimal mass and, thus, does not influence the orbits of the Earth and the Moon. A rotating frame based in the motion of the primaries is adopted to describe the behavior of the spacecraft governed by the two bodies. In this frame, represented $\{\hat{x},\ \hat{y}, \hat{z}\}$, $\hat{x}$ is directed from the Earth to the Moon, $\hat{z}$ is parallel to the angular momentum direction of the system, and $\hat{y}$ completes the dextral orthonormal triad. The quantities $l^*,\ m^*$, and t^*, termed the characteristic length, characteristic mass, and characteristic time, respectively, nondimensionalize the equations of motion of the spacecraft in this model.[3] The resulting scalar equations of motion that represent the motion of the spacecraft as expressed in the rotating frame are expressed as,

$$\ddot{x} - 2\dot{y} = \frac{\partial U^*}{\partial x}, \quad \ddot{y} + 2\dot{x} = \frac{\partial U^*}{\partial y}, \quad \ddot{z} = \frac{\partial U^*}{\partial z} \tag{1}$$

The quantity U^* is the pseudo-potential function, determined as,

$$U^* = \frac{1-\mu}{r_{13}} + \frac{\mu}{r_{23}} + \frac{x^2+y^2}{2} \tag{2}$$

where μ is the system mass parameter evaluated as $\mu = \frac{M_2}{M_1+M_2}$, with M_1 and M_2 representing the mass of the Earth and the Moon, respectively. Additionally, r_{13} and r_{23} denote the nondimensional distances between the Earth and the spacecraft as well as the Moon and the spacecraft, respectively. The values (x, y, z) correspond to the nondimensional position of the spacecraft relative to the system barycenter in the Earth-Moon rotating frame; similarly, $(\dot{x}, \dot{y}, \dot{z})$ represent the velocity components of the spacecraft as viewed in the rotating frame. While a closed-form solution does not exist for the equations of motion in the CR3BP, the model permits one integral of the motion, termed the Jacobi constant and evaluated as $C = 2U^* - v^2$, where v is the speed of the spacecraft relative to the rotating frame. The Jacobi constant is inversely proportional to the energy of the system and remains constant for ballistic propagation in the CR3BP. There exist five equilibrium solutions in the CR3BP, termed the libration points and denoted L_i for $i = 1, 2, ..., 5$. Of these libration points, L_1 and L_2 lie approximately $57,000\ km$ and $63,000\ km$ from the surface of the Moon, respectively. Considering the vastness of cislunar space, the proximity of these points to the Moon has prompted the exploration of dynamical structures in their vicinity to enable lunar exploration.[4] One type of such a dynamical structure includes periodic orbits constructed in the CR3BP. There exist

periodic orbits that traverse the vicinity of the libration points, as well as orbits in the neighborhoods of the primaries in the rotating frame. Additionally, the existence of a single periodic orbit leads to the determination of a family of periodic orbits, typically characterized by similar geometries that evolve in Jacobi constant value. Thus, rather than assessing isolated trajectories, the wide range of similarly characterized orbits supply additional options for viable trajectories for mission design.

CR3BP Resonant Orbits

A particularly useful option for periodic orbits in the CR3BP includes orbits that are resonant with the lunar sidereal period ($T_{sid} = 27.32\ days$). When analyzed in the CR3BP rotating frame, these orbits, hereby denoted resonant orbits, exhibit expansive geometries that sweep through broader areas of cislunar space. Such orbits are characterized by their resonance ratio, denoted p:q, that is a simple integer ratio of the orbital period of the Moon and the spacecraft orbit. A spacecraft in a p:q resonance with the Moon encircles the Earth p times in the interval required for the Moon to complete q revolutions of the Earth. For resonant orbits constructed in the Earth-Moon CR3BP, the ratio of the orbital periods may not necessarily be integer. As such, a spacecraft in p:q resonance constructed in this model completes p orbits in *approximately* the time required for the Moon to complete q orbits around the Earth. Nonetheless, such orbits are precisely periodic in the rotating frame. For an integer resonance ratio of p:q, orbits with $p > q$ are denoted interior resonant orbits. The periods of these orbits, as viewed in the inertial frame, are shorter than the period of the Moon. In general, these orbits remain interior to the Earth-Moon system. Alternatively, when $p < q$, the orbits are termed exterior resonant orbits. The orbital periods in this case are longer than the period of the Moon, and the orbits provide excursions beyond the Earth-Moon system, with potential opportunities for close periodic passes of the two bodies.

As is true for all periodic solutions in the CR3BP, the construction of a single resonant orbit in this model guarantees the existence of a family of resonant orbits. Although the orbits in the family exist over a range of periods and, as a result, are *nearly resonant*, they exhibit resonant behavior and characteristics that retain the utility of the underlying sidereal resonant orbits. The construction of planar resonant orbit families enables the search for three-dimensional resonant orbit families that provide excursions beyond the Earth-Moon plane. The availability of such solutions opens additional dynamically viable regions for spacecraft pathways over various values of the Jacobi constant. To construct spatial families of resonant orbits, the eigenvalue structure of the monodromy matrix along the planar orbit families is investigated in search of bifurcating orbits.[5] In the current work, certain tangent and period-doubling bifurcations from planar resonant families are identified to construct their spatial analogs. Families of planar and spatial resonant orbits corresponding to various resonance ratios appear in Figure 1, where orbits are colored by their Jacobi constant values for each ratio. The orbits in black highlight the direction of motion along the trajectory, indicated via black arrows. Also plotted in Figure 1 is the evolution of the stability index and the orbit period along each resonance family. The stability index is a function of the eigenvalues (λ_j) of the monodromy matrix for each resonant orbit and is determined as $\nu_j = \frac{1}{2}\left(||\lambda_j|| + \frac{1}{||\lambda_j||}\right)$. The stability index provides a measure of the linear instability of each orbit, where a value greater than unity indicates that the orbit is unstable in a linear sense.[6] In addition to the stability index, the evolution of the orbit periods in the CR3BP (i.e., the period in the rotating frame), appear in red along the right vertical axes for each family. Overall, the planar and spatial orbit families illustrate vastly differing geometries and stability properties spanning various energy levels. This characteristic of resonant orbits renders them particularly useful for trajectory design in the cislunar

domain, since access to various regions within this space is available via their expansive geometries and energy range.

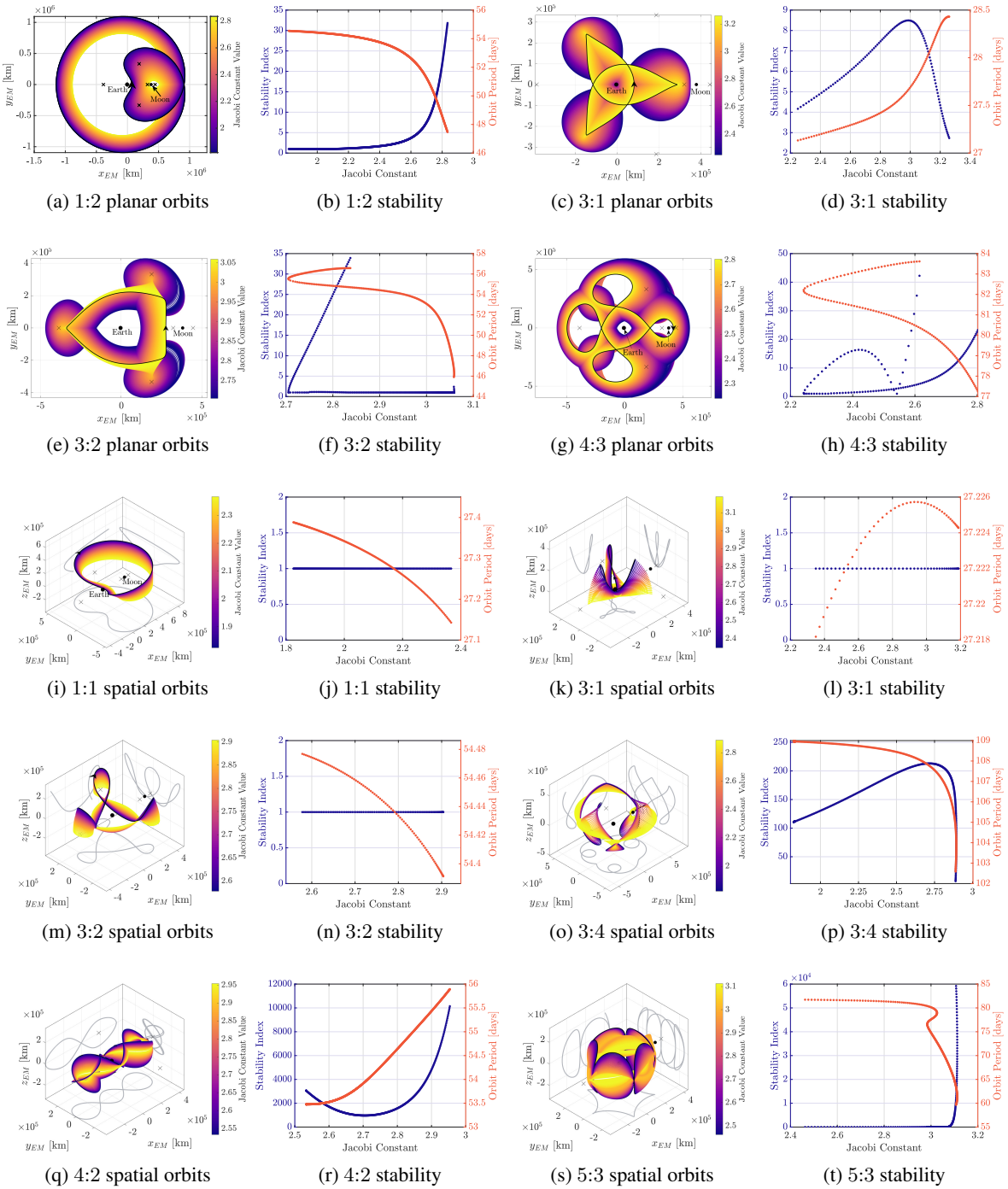

(a) 1:2 planar orbits (b) 1:2 stability (c) 3:1 planar orbits (d) 3:1 stability

(e) 3:2 planar orbits (f) 3:2 stability (g) 4:3 planar orbits (h) 4:3 stability

(i) 1:1 spatial orbits (j) 1:1 stability (k) 3:1 spatial orbits (l) 3:1 stability

(m) 3:2 spatial orbits (n) 3:2 stability (o) 3:4 spatial orbits (p) 3:4 stability

(q) 4:2 spatial orbits (r) 4:2 stability (s) 5:3 spatial orbits (t) 5:3 stability

Figure 1. Families of resonant orbits constructed in the Earth-Moon CR3BP and plotted in the rotating frame.

Resonant Orbits with Sidereal-Synodic Overlap

For certain sidereal resonant orbit families in the CR3BP, it is possible to identify members that, in addition to being nearly sidereal resonant with the Moon, exhibit lunar synodic resonance as well. This characteristic arises due to the orbits being *nearly* sidereal resonant, a characteristic that allows the family of sidereal resonant orbits to span a wide range of orbital periods in the rotating frame. Thus, the orbits retain favorable geometries and stability properties inherent to their sidereal resonant structure, with the added advantage of repeatability relative to the orientation of the Sun in the Earth-Moon rotating frame. This characteristic is particularly relevant for SSA operations beyond the vicinity of the Earth, where illumination and visibility conditions are evaluated.[7] The synodic resonance also renders these orbits favorable for eclipse avoidance where, depending upon the resonance ratio, options for multiple baseline trajectories are available that naturally avoid the shadows cast by the Earth and the Moon.[8]

Sample orbits from various sidereal resonant families that are commensurate with the lunar synodic period in the rotating frame are identified in Figure 2. Figures 2(a), 2(c), 2(e) and 2(g) represent synodic resonant members from the 1:2, 2:1, 4:3, and 2:1-H_1 sidereal resonance families, respectively. In each plot, the legend indicates the ratio of the associated synodic resonance. For reference, Figures 2(b), 2(d), 2(f) and 2(h) represent the ratio of the lunar synodic period ($T_{syn} = 29.53\ days$) with the period along the family for the associated sidereal resonant orbits. Integer ratios from these plots are identified, yielding several options for orbits that exhibit the sidereal-synodic overlap. However, for practical purposes, it is useful to focus on the orbits that exhibit a smaller resonance order, since those members tend to possess shorter periods in the rotating frame. Notably, this synodic resonance allows the orbits to provide repeatability with respect to the Earth-Moon-Sun orientation, while preserving the geometry that is unique to sidereal resonant behavior.

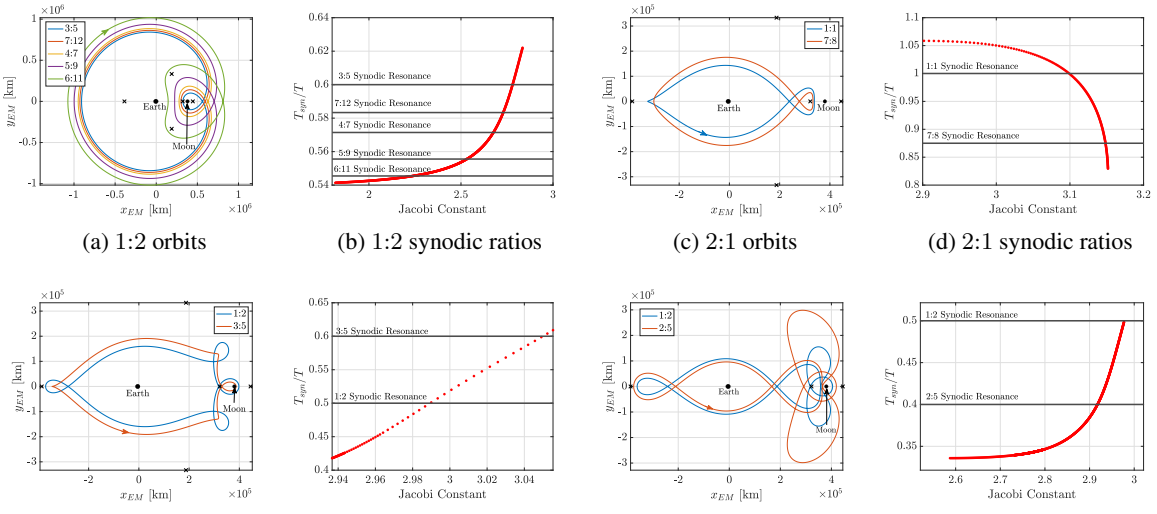

(a) 1:2 orbits (b) 1:2 synodic ratios (c) 2:1 orbits (d) 2:1 synodic ratios

(e) 4:3 orbits (f) 4:3 synodic ratios (g) 2:1-H_1 orbits (h) 2:1-H_1 synodic ratios

Figure 2. Orbits from various sidereal resonant families that are commensurate with the lunar synodic period.

OBSERVING TARGETS IN CISLUNAR SPACE

To establish a comprehensive SSA architecture in cislunar space, the need for space-based sensors has been recognized.[9,10] With the availability of unique vantage points across the cislunar domain, space-based sensors enable the detection and tracking of objects in space, especially beyond GEO and in the vicinity of the Moon. Observations from space-based sensors are key for supporting autonomous navigation, communications, and sustaining operations beyond the Earth. For optical sensors operating in space, there also exist inherent limitations that may curtail the visibility of targets of interest. These challenges include insufficient illumination of the target object that limit the frequency with which targets are visible to the observer spacecraft.[7] These conditions for evaluating the visibility of a target as viewed by space-based optical observers are detailed within the context of cislunar space.

Limiting Apparent Magnitude

In astronomy, the apparent magnitude is a measure of the brightness of an object.[7,11] The apparent magnitude of a target as seen by an observer is critical in determining the brightness and, by extension, the nature of a target as "visible".[12] The magnitude of an object is evaluated as,

$$m_T = m_S - 2.5 \log \left[\frac{2\, C_d\, R_T^2}{3\, \pi^2\, r_{OT}^2} \left(\sin\psi + (\pi - \psi) \cos\psi \right) \right] \tag{3}$$

where C_d is the reflection parameter for the target and R_T is the radius of the target, i.e., an indicator of its size. The angle ψ is the Sun-target-observer angle and is termed the solar phase angle. Finally, the quantity m_S is the apparent magnitude of the Sun and is fixed as -26.74. The magnitude scale is reverse logarithmic: a lower value of the magnitude is indicative of a brighter object. For reference, Figure 3(a) illustrates the orientation of the target relative to the Sun and the observer and the associated angle definitions. The utility of any space-based observer may be assessed by quantifying the brightness of various targets as they appear to the observer, and assessing the value to determine if it is less than some limiting magnitude. The reference limiting magnitude values employed by various authors are detailed in Table 1. While this limiting magnitude is inherently a function of the sensor aperture and the properties of the detector, in the current work, a representative value of $m_{\lim} = 20$ is employed to yield a broad evaluation of the observer performance. For further analysis and, to accommodate various optical sensor apertures, lower values of the limiting magnitude may be explored. Thus, when a target possesses a magnitude less than $m_{\lim}$, it is assumed to be visible to the observer. In this investigation, all targets are characterized as Lambertian spheres with a $R_T = 3.54\ m$ and a diffuse reflection coefficient equal to $C_d = 0.5$.[11] Finally, since the Earth-Moon CR3BP is the primary dynamical model in this investigation, the magnitude of each target is directly evaluated in the Earth-Moon rotating frame, with the position of the Sun obtained via the SPICE Toolkit and transformed directly into this frame.[13]

Exclusion Zone Modeling

For targets that lie close to the line-of-sight with the Sun, the Earth, or the Moon, the brightness of the celestial body causes the target to be backlit as viewed by the observer. As such, any onboard optical sensors may not be able to obtain or maintain custody of the target, assuming solely optical measurements are incorporated. To identify the severity of this effect, exclusion zones are defined for each body. These conical zones, such as the solar exclusion zone depicted in Figure 3(a), are centered on the observer and expand out towards the celestial body. The exclusion angle, denoted

Table 1. Reference values for limiting apparent magnitude.

Authors	Limiting Magnitude
Thompson et al.[9]	$13 - 16$
Frueh et al.[11,14]	20
Bhadauria et al.[7]	20
Vallado et al.[12]	$16.5 - 17.5$
Worthy et al.[15]	$12 - 15$
Vendl et al.[16]	$17 - 20$
Current work	20

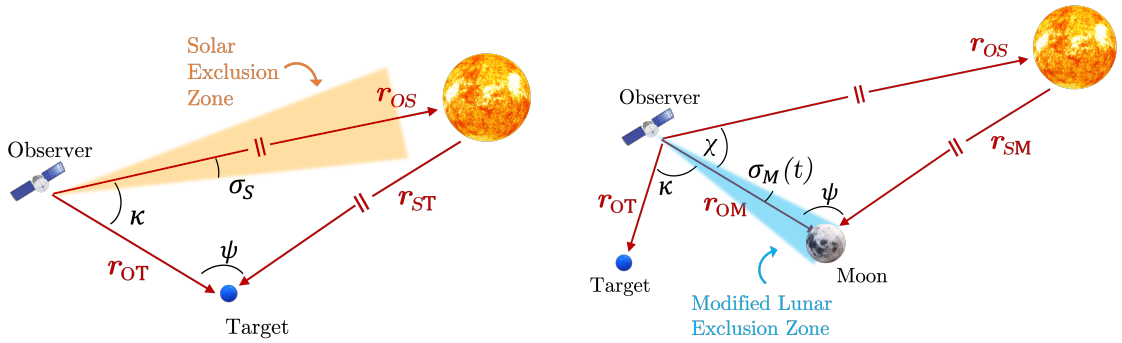

(a) Sun-target-observer geometry

(b) Lunar exclusion modeling

Figure 3. Schematics for the Sun-target-observer geometry and relevant exclusion zones.

σ_i, is the cone half-angle that defines the exclusion zone cast by the body. The angle κ locates the target relative to the axis of the exclusion zone, as defined in Figure 3(a), and varies as the relative positions of the observer, target, and the Sun change with time. For a target to be visible in space, then, the following exclusion condition is defined,

$$\kappa(t) > \sigma_i \tag{4}$$

where σ_i represents the exclusion angle for each of the three bodies. The solar exclusion angle is represented as σ_S, σ_E represents the Earth exclusion angle, and σ_M defines the lunar exclusion zone. Table 2 summarizes exclusion angles employed by various authors, as well as the values in this investigation. For a target to be visible to the observer at any time, Equation (4) must be satisfied for exclusion resulting from all three celestial bodies at that time.

For challenges with solar exclusion, the long range between the Sun and the observer (and target) is leveraged to inform a solar phase angle that minimizes exclusion. From Figure 3(a), it is apparent that,

$$\kappa + \psi \approx 180^\circ \tag{5}$$

When $\kappa \leq \sigma_S$, the target lies within the solar exclusion zone and is not visible to the observer. Thus, a relative phasing between the observer and target is desired such that $\psi \in [0, 180 - \sigma_S]$.

By phasing the observer appropriately, the impact of solar exclusion on the visibility of a target is reduced.

Table 2. Reference values for exclusion angles.

Authors	Solar Exclusion [deg]	Earth Exclusion [deg]	Lunar Exclusion [deg]
Thompson et al.[9]	30	10	10
Bhadauria et al.[7]	50	35	30
Vallado et al.[12]	30	-	10
Fowler et al.[17]	30	-	-
Kinzly et al.[18]	10	10	10
Somavarapu et al.[19]	15	-	-
Current work	30	10	10

Modified Lunar Exclusion Zone

For targets in cislunar space and, in particular, those that exist in the vicinity of the Moon, lunar exclusion significantly impacts visibility.[9] While the nominal value for the lunar exclusion zone defined in Table 2 aids preliminary analyses, one methodology for increasing the fidelity of modeling the lunar exclusion zone considers the brightness of the Moon itself. Depending upon the lunar phase as viewed by the space-based observer, the Moon may appear full (i.e., brightest), or new (i.e., dimmest). Intuitively, this cycle is equivalent to the phases of the Moon as seen from the Earth every lunar synodic period. During a full Moon event as viewed by the observer in space, the target will be completely backlit. As such, any exclusion due to the Moon is maximized, and $\sigma_M(t) = \sigma_M = 10^\circ$. Conversely, during a new Moon, the Moon is the dimmest as viewed by the observer, and $\sigma_M(t) = 0^\circ$. Based on the lunar phase viewed by the observer at any time, then, the modified lunar exclusion zone is defined as a function of the lunar phase angle, denoted $\chi(t)$, and illustrated in Figure 3(b). The case of $\chi(t) = 0^\circ$ occurs when Moon lies between the observer and the Sun and causes no exclusion; when $\chi(t) = 180^\circ$, the Sun-observer-Moon orientation occurs and results in maximum lunar exclusion. Based on the value of $\chi(t)$ for every time step, the lunar exclusion zone angle is instantaneously determined as,

$$\sigma_M(t) = 10^\circ \cdot \frac{\chi(t)}{180^\circ} \tag{6}$$

where $\chi(t)$ is measured in degrees, and the value 10° is the standard, constant lunar exclusion angle defined in Table 2. Equation (6), then, essentially scales the nominal value of the lunar exclusion angle based on the brightness of the Moon, increasing the fidelity of modeling lunar exclusion.

MODELING TARGET LOCATIONS

While it is not possible to uniquely examine the visibility at every point in cislunar space, a representation of the quality of an observer trajectory is assessed by determining the visibility of various targets. To evaluate the ability of an observer to track various locations within cislunar space, the following three scenarios for modeling target locations are examined:

- **Targets within the Lunar Exclusion Cone (LEC)**:
  For a given solar phase, the illumination of the Moon may be such that Earth ground-based observations of a target located between the Earth and the Moon may not be possible due to lunar exclusion. As such, this conical volume centered on the Earth and facing out towards the Moon is identified as a high priority zone for maturing the current tracking and surveillance capabilities in cislunar space.[20] As a conservative estimate, a fixed cone with a 30° half-angle is used to define this zone, also called the "cone of shame".[20] In this investigation, this region is denoted the Lunar Exclusion Cone (LEC). Targets are randomly sampled from a uniform distribution of points in this cone to represent the underlying volume of space. The current work assumes the length of the LEC to equal $500,000\ km$, extending just beyond the the L_2 libration point. Figure 4(a) illustrates a sample distribution of targets located in the LEC.

- **Targets within the cislunar domain**:
  It is also possible to randomly sample various target locations across the entire volume of the cislunar domain. Only the knowledge of the target positions is assumed. But, depending upon their velocity, targets may be able to rapidly access other locations of interest, thus, rendering these locations equally important for visibility assessment. Figure 4(b) illustrates a sample distribution of targets distributed across the spherical volume of cislunar space. In the current work, the radius of this sphere is equal to $500,000\ km$ and encompasses all the libration points.

- **Targets operating in cislunar orbits**:
  The knowledge of existing periodic orbits in the Earth-Moon CR3BP also offers insight into the possible locations of targets. By considering targets operating in various periodic orbits, the knowledge of their velocity at a given energy level is also available. In this investigation, five representative targets are employed that operate independently near the L_1, L_2, L_4, and L_5 libration points. For the L_1 and L_2 cases, the targets are modeled in halo orbits about these points. For the targets about L_4 and L_5, planar Short Period Orbits (SPOs) are employed as representative examples. An additional target is assumed to operate in a spatial Distant Retrograde Orbit (DRO). These five sample target orbits are visualized in Figure 4(c) in the Earth-Moon rotating frame. The visibility of any number of the five possible target orbits is evaluated.

The first two scenarios represent the *probable* locations of targets in cislunar space, whereas the third approach is guided by the *possible* locations of targets. By determining their apparent magnitudes and orientation relative to cislunar exclusion zones, the visibility of each target location for the detailed scenarios is assessed by constructing various observer trajectories in the Earth-Moon CR3BP. The following conditions determine the visibility of each target from the observer spacecraft:

1. The apparent magnitude of the target is less than the limiting magnitude.
2. The target lies outside the solar exclusion zone.
3. The target lies outside the Earth exclusion zone.
4. The target lies outside the modified lunar exclusion zone.

These metrics, along with the three scenarios for modeling target locations in cislunar space, provide a baseline assessment of the utility of the considered observer orbits for supporting cislunar SSA.

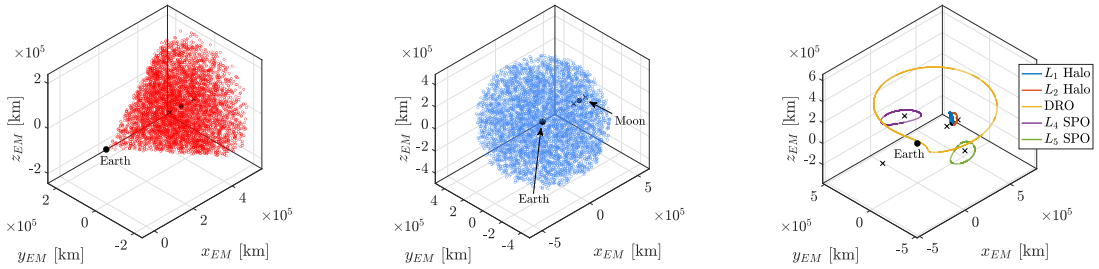

(a) Targets in the LEC (b) Targets in the cislunar domain (c) Targets in cislunar orbits

Figure 4. Sample target representations identified within various regions in cislunar space.

EXAMPLE: SINGLE OBSERVER IN A SIDEREAL-SYNODIC RESONANCE

To demonstrate the assessment of visibility conditions for various targets in cislunar space, along with the advantages of geometries supplied by sidereal resonant orbits, resonant orbits with sidereal-synodic overlap are explored. Specifically, a representative example follows an optical observer operating in the 1:1 synodic resonant member from the family of 2:1 sidereal resonant orbits identified in Figure 2(c). Given that both favorable and unfavorable visibility conditions repeat with the lunar synodic period, the choice of this synodic resonant orbit enables the identification of ideal conditions for observers tasked with tracking targets. In the subsequent analysis, an initial epoch corresponding to January 01 2025 00:00:00 UTC is assumed to locate the Sun in the Earth-Moon rotating frame.

Visibility of Targets in the LEC

The efficacy of an observer operating in the 1:1 synodic resonant member from the 2:1 sidereal resonant family is assessed for targets located inside the Lunar Exclusion Cone (LEC). As an example, $5,000$ points are randomly distributed inside the cone defined by the LEC, as illustrated in Figure 4(a). The targets are stationary, and there is no assumed knowledge of their velocity. Thus, as the observer spacecraft moves along its orbit, the visibility at locations represented by the fixed targets is evaluated. At each sampled instance in time, the percentage of targets that meet the criteria for visibility is recorded. Figure 5 illustrates the visibility of each target point within the LEC at the initial time, when the observer in the blue orbit is located at apolune. At this instant in time, the targets highlighted in green in Figure 5 represent the volume of the LEC that is visible to the observer for the associated visibility criterion. Clearly, the limiting case at this time is solar exclusion, with only 2% of the volume visible due to solar backlighting. Comparatively, the percentage of the volume with a visible apparent magnitude is 34%, the volume outside Earth exclusion is 58%, and outside the lunar exclusion zone is 96%.

This process of observing the LEC from different locations along the sidereal-synodic resonant orbit is repeated for twelve instances along the observer orbit over one revolution in the rotating frame. At each of the twelve locations, the percentage of the volume of the LEC that is visible to the observer from each of the sampled time steps is recorded. The results over one synodic period appear in Figure 6, where the vertical axes represent the percentage of targets that are visible to the observer at the sampled time step along the orbit and, thus, representing the percentage of the volume of the LEC that is visible. Intuitively, as the observer approaches the vicinity of the Moon

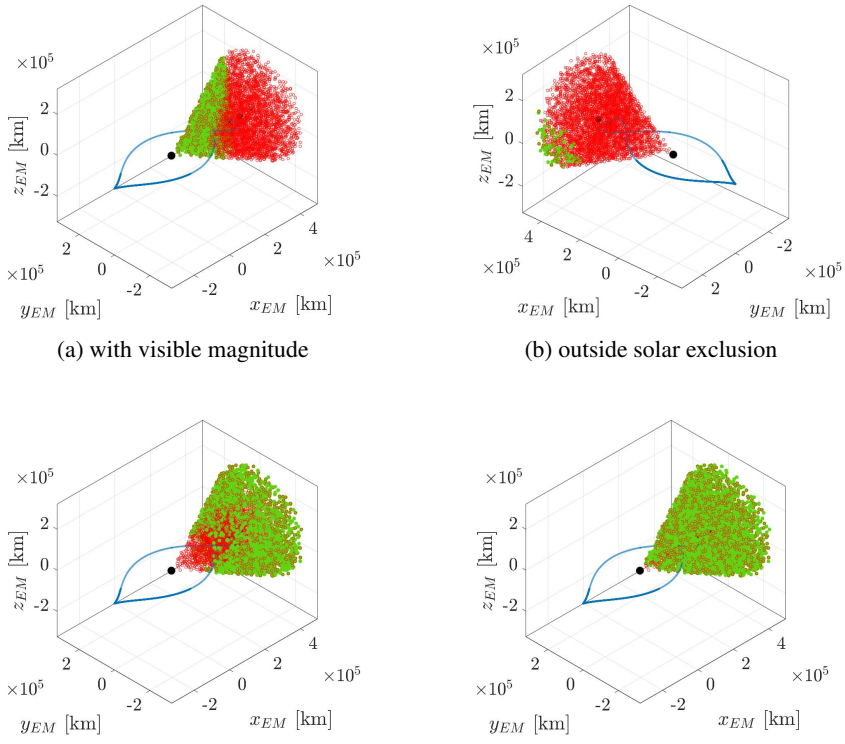

(a) with visible magnitude

(b) outside solar exclusion

(c) outside Earth exclusion

(d) outside lunar exclusion

Figure 5. Visibility of fixed-position targets in the LEC as viewed by the 1:1 synodic resonant observer at initial time.

(after traversing through the vicinity of the Earth), the number of visible targets increases. The phasing of the observer and the Moon is such that when the observer is at the half-period mark (near L_2), the Sun is located towards L_3; thus, solar exclusion effects also reduce. When the observer is far from the Moon, lunar exclusion does not occur; when the observer is close to the Moon, the Sun-Moon-observer phasing is such that lunar exclusion is minimized. Notably, since this orbit is in 1:1 synodic resonance with the Moon, the visibility of targets over one revolution persists over subsequent revolutions as well. In general, this behavior demonstrates the advantages of resonant orbits for hosting space-based optical sensors, as the challenges with geometries that inhibit illumination are alleviated via their unique vantage points that manifest under natural dynamics.

Visibility of Targets in the Cislunar Domain

The same analysis is repeated for the cislunar domain as defined in Figure 4(b). As a representative example, $5,000$ points are sampled from this volume to represent stationary targets that are dispersed throughout cislunar space. At the initial time, when the observer is located at apolune, the targets that meet the various visibility criteria are highlighted in green in Figure 7. While solar exclusion still restricts the visibility of targets, fewer targets meet the limiting magnitude criterion at this time step. Only 73% of the targets possess an apparent magnitude that is lower than the limiting value; 77% of the targets are outside the solar exclusion zone. In this scenario, Earth and lunar exclusion do not significantly impact the visibility of targets, considering that a majority number of

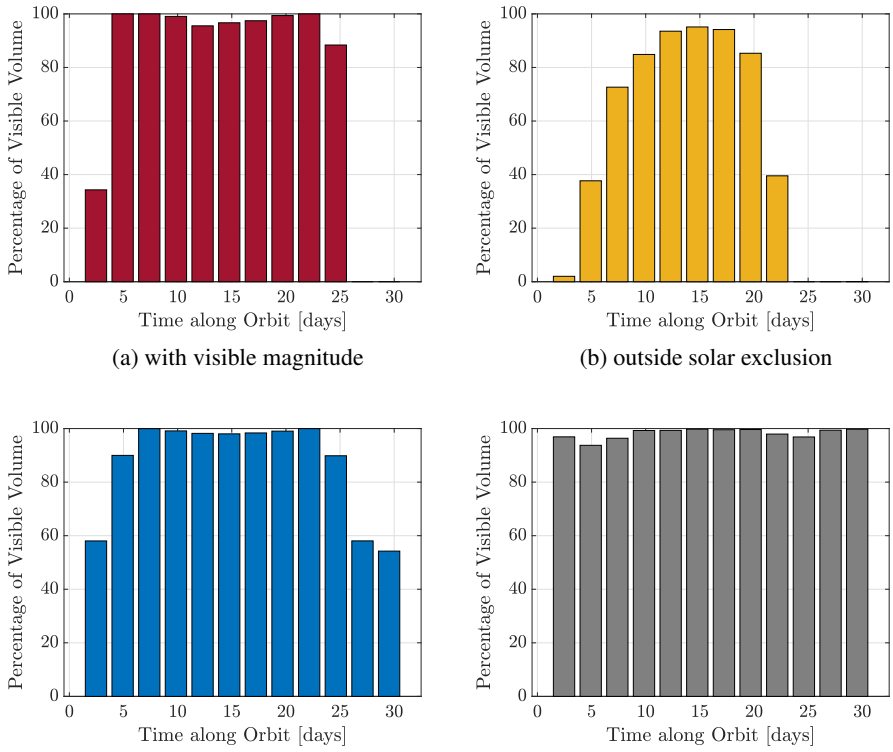

(a) with visible magnitude

(b) outside solar exclusion

(c) outside Earth exclusion

(d) outside lunar exclusion

Figure 6. Overall visibility of fixed-position targets in the LEC as viewed by the 1:1 synodic resonant observer over one month.

targets lie significantly beyond the Earth-Moon plane.

Propagating the observer in its orbit changes the orientation of the observer spacecraft relative to the Sun and the fixed-position targets that describe the cislunar domain. As a result, at subsequent time steps, a greater percentage of the volume becomes visible to the observer. The number of targets that are visible to the observer under various conditions appear in Figure 8. In general, the volume is well observed in the presence of solar, Earth, and lunar exclusion zones. The limiting magnitude is the predominant factor that restricts the visibility of the targets. However, it is noted that the number of targets visible to the observer in Figure 8(a) oscillates with the solar phase angle. Thus, to mitigate the challenges with illumination imposed by the limiting magnitude, multiple observers may be incorporated such that their phase is offset from the solar phase angle.

Visibility of Targets in Cislunar Periodic Orbits

The final scenario for assessing the quality of an observer orbit for optical observations of cislunar space is by evaluating the targets in the representative periodic orbits illustrated in Figure 4(c). The initial conditions employed in the previous two scenarios are assumed for the observer, with the spacecraft located at apolune and the Sun oriented at the epoch January 01 2025 at initial time. The observer, and the targets in their orbit, are propagated for one synodic period and appear in Figure 9(a) as viewed in the Earth-Moon rotating frame. Figure 9(c) illustrates the apparent magnitude of each target as viewed by the observer over the propagated synodic period, where the black line

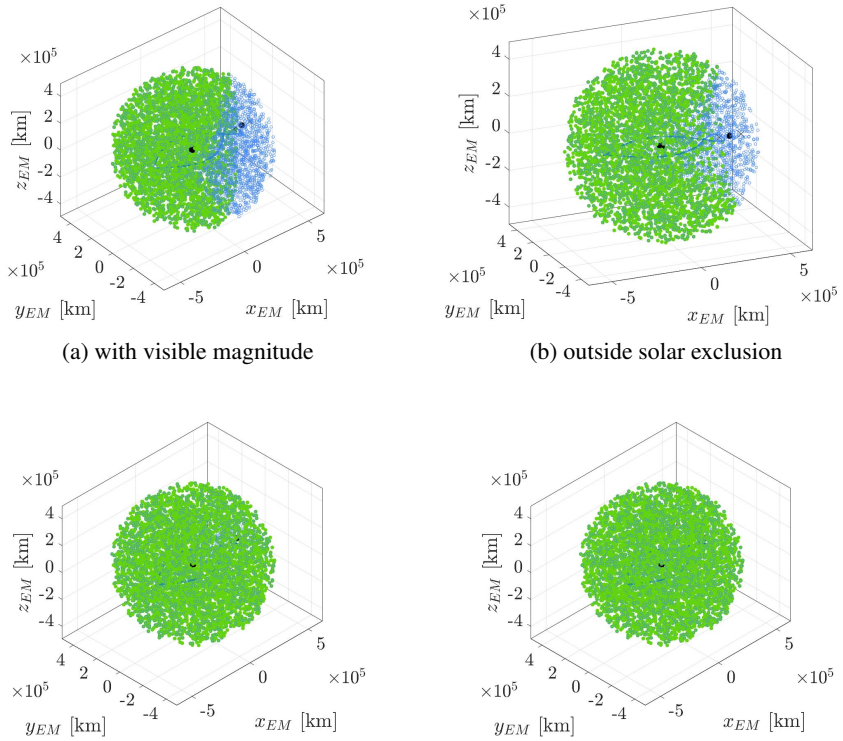

(a) with visible magnitude

(b) outside solar exclusion

(c) outside Earth exclusion

(d) outside lunar exclusion

Figure 7. Visibility of fixed-position targets in the cislunar domain as viewed by the 1:1 synodic resonant observer at initial time.

indicates the limiting magnitude. Considering all the visibility conditions together, the number of days that each target is visible to the observer are summarized in Table 3. Evidently, solar exclusion is the predominant issue that inhibits visibility for all the planar targets. This result is intuitive, since all the objects lie in the same plane as the solar exclusion zone. In addition to the higher magnitude values for the libration point orbits in Figure 9(c), passage through the solar exclusion zone limits their visibility.

Table 3. Visibility of targets in cislunar orbits for one period of the 1:1 synodic resonant orbit. The phasing of the observers and the targets assumes an initial epoch of January 01 2025.

Target Orbit	Number of Days Visible
L_1 Halo	18.5
L_2 Halo	16.9
DRO	27.9
L_4 SPO	14.7
L_5 SPO	14.3

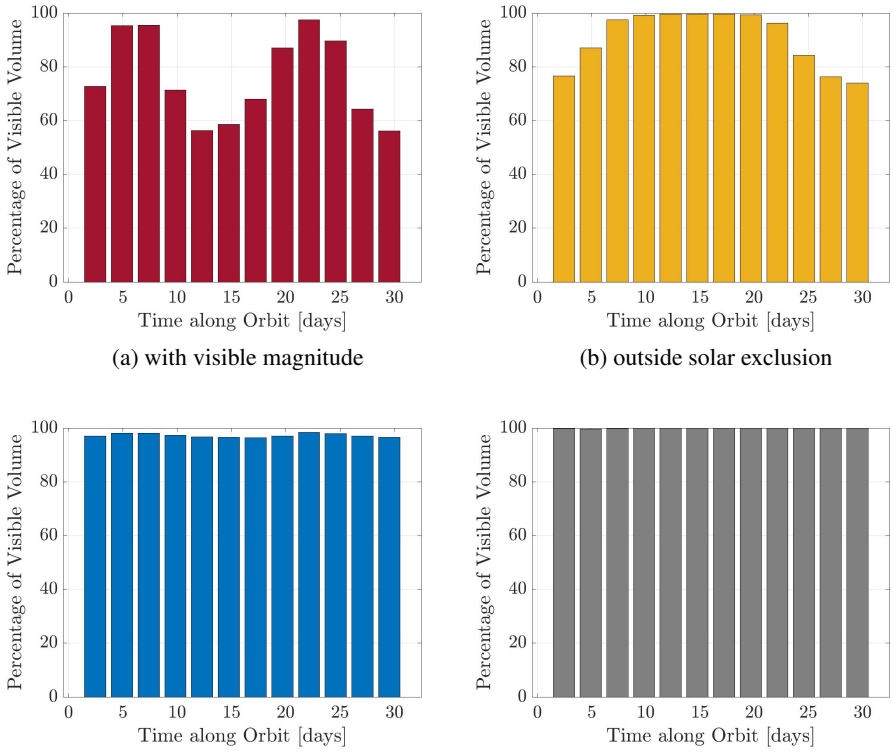

(a) with visible magnitude

(b) outside solar exclusion

(c) outside Earth exclusion

(d) outside lunar exclusion

Figure 8. Overall visibility of fixed-position targets in the cislunar domain as viewed by the 1:1 synodic resonant observer over one month.

Observer Phase Modification

One option for mitigating the challenges of a sensor's limiting magnitude is to vary the relative phasing for the observer and the target. Without any modifications to the target in its orbit, and with the initial location of the observer fixed at apolune, the epoch is allowed to vary. This change in epoch induces a variation in the solar phase angle, allowing the identification of an observer phasing that is better suited for optical observations of the target. Recall that the observer is located in a 1:1 synodic resonant member from the 2:1 sidereal resonant periodic orbit family constructed in the Earth-Moon CR3BP. This process is illustrated in Figure 10, where the magnitude and solar phase angle for each target are evaluated over a range of epochs. In each magnitude plot in Figure 10, the black line indicates the limiting magnitude employed in the current work. In the plots representing the solar phase angles, the black line is indicative of the requirement on the solar phase angle recognized in Equation (5): when the solar phase angle exceeds $180 - \sigma_S = 150°$, the condition recognized in Equation (5) is violated, and the target is not visible to the observer. Thus, in each solar phase plot in Figure 10, the target will not be visible to the observer when the angle exceeds the indicated solid black line. The inverse relationship between the magnitude and the solar phase angle is apparent. Regions of low magnitude, that are indicative of visible targets, correspond to low solar phase angles. The optimal phasing scenario occurs for the target in the DRO illustrated in Figure 10(c). Here, in the minimum magnitude case (yellow), the timing of the locations of the highest magnitude coincide with the passage of the target through the solar exclusion zone. This

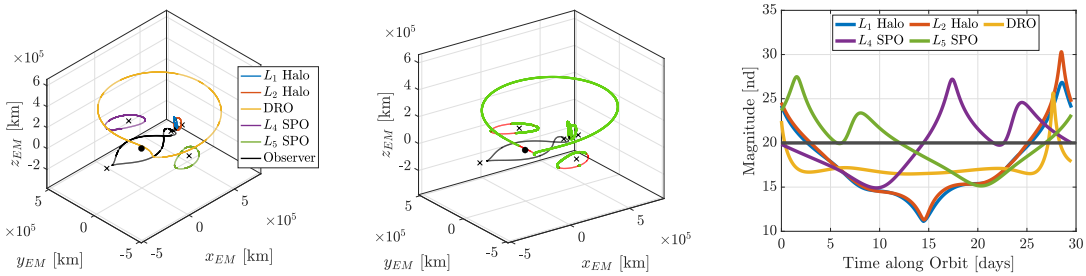

(a) Observer and target orbits (b) Visibility of each target orbit (c) Apparent magnitude of each target

Figure 9. Visibility of targets in various periodic orbits as viewed by the 1:1 synodic resonant observer.

configuration yields the ideal visibility conditions for the target as viewed from the observer in the given resonant orbit. Notably, due to the synodic resonance of the observer orbit, these ideal visibility conditions persist over subsequent revolutions as well.

EXAMPLE: CONSTELLATION OF OBSERVERS IN A SIDEREAL-SYNODIC RESONANCE

The vastness of cislunar space limits the abilities of single observer spacecraft to adequately surveil this space over time. As demonstrated via the single-observer example, the effects of solar exclusion, in particular, restrict the visibility of targets throughout the cislunar volume. However, the properties of sidereal resonant orbits that are in synodic resonance with the Moon provide options for phasing multiple observers in the same underlying resonant orbit to supply comprehensive coverage. As an example, a 2:5 synodic resonant orbit from the family of 5:3 spatial sidereal resonant orbits is selected.[8] Although there exist options for synodic resonant orbits with shorter periods, this orbit traverses the cislunar volume spatially, providing additional vantage points for observations and visibility beyond the Earth-Moon plane. The longer orbital period also allows the observer spacecraft to be spaced sufficiently far away from the other observers in the network to achieve broader coverage. The spatial geometry of the orbit is also favorable for achieving line-of-sight with assets on the lunar far-side.

Table 4. Characteristics of the selected sidereal resonant orbit with a synodic overlap.

Parameter	Value
Jacobi Constant	3.0127
Period [days]	73.81
Maximum Spatial Excursion [km]	91,040
Perilune Altitude [km]	69,000

A sample constellation of multiple space-based observers operating in the 2:5 synodic resonant orbit is designed. Comprehensive surveillance could, in such a scenario, be achieved by phasing the sensors such that they pass through different regions of cislunar space at the same time. From an operations standpoint, this architecture offers redundancy in cislunar coverage, since a volume that is swept by one observer is revisited by the other observers in the network. Additionally, depending upon the selection of the primary orbit, concerns regarding communications with the Earth may be

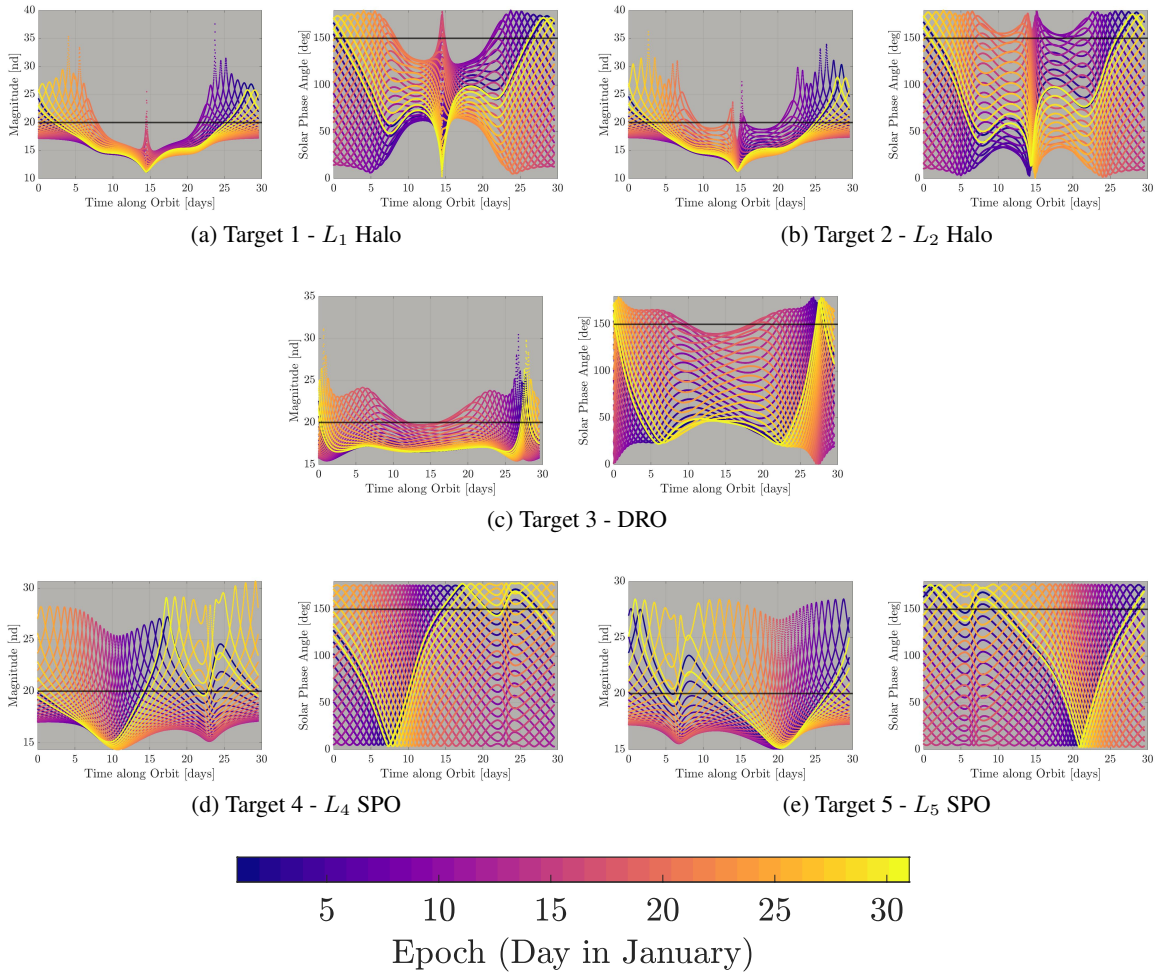

(a) Target 1 - L_1 Halo

(b) Target 2 - L_2 Halo

(c) Target 3 - DRO

(d) Target 4 - L_4 SPO

(e) Target 5 - L_5 SPO

Figure 10. Change in the apparent magnitude for various targets over one synodic period as a function of the initial Sun-observer orientation.

alleviated. In contrast to a spacecraft located behind the Moon, all observers in the network have the opportunity to directly interface with Earth-based ground stations.

As an example, four space-based observers are located in this orbit. For resonant orbits, a natural choice for the initial phasing of the observers is the locations of apses or, in the Earth-Moon rotating frame, along the loops around the orbit. Two observers are initially placed at two of the four periapses along the orbit that appear on either side of the Earth. The remaining two are located at two of the four apoapses relative to the Earth, one near L_3 and the other at the orbit perilune. Figure 11 illustrates the four observers at their initial locations along the orbit as viewed in the Earth-centered inertial and Earth-Moon rotating frames. Note that in the Earth-centered inertial frame, two of the observers (blue and red) appear overlaid due to the coincidence of periapses at the initial time, exaggerated by the marker size. The visibility of various targets is assessed over one rotating frame period of each observer in this orbit, or for approximately 74 $days$.

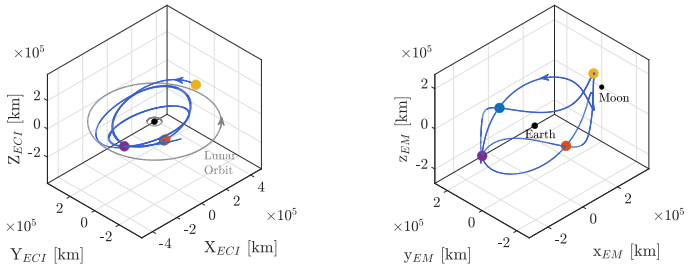

(a) Earth-centered inertial frame (b) Earth-Moon rotating frame

Figure 11. Initial locations of four observers phased along the 2:5 synodic resonant orbit in the CR3BP as seen in the Earth-centered inertial and Earth-Moon rotating frame.

Visibility of Targets in the LEC

While each observer independently may not be able to sufficiently observe the entire volume of the Lunar Exclusion Cone (LEC) at a given instant in time, together, the constellation provides comprehensive visibility of this target volume. On the whole, considering visibility due to the limiting magnitude, solar, Earth, and lunar exclusion, over 90% of the targets are visible to at least one observer at each time. Solar exclusion remains the predominant issue in limiting the visibility of this volume from space-based observers; however, the observer phasing in the constellation is such that the visibility of targets in this region is significantly improved compared to a single-observer scenario. Additionally, as the observers go along the orbit in time, redundancy in optical observations of the same target is also supplied.

Visibility of Targets in the Cislunar Domain

Overall, the spherical volume that defines the cislunar domain in this investigation is well observed by the space-based observers in this constellation. At each instant in time, over 96% of the targets defined in Figure 4(b) are visible to at least one observer in the constellation. The observers provide various vantage points that, together, overcome the issues in visibility faced by the single-observer case.

Visibility of Targets in Cislunar Periodic Orbits

Finally, the visibility of cislunar targets in the representative orbits introduced in Figure 4(c) is assessed for the observers in the constellation. In Figure 12, each plot illustrates the apparent magnitude for all the targets in their orbits as viewed by each observer for the given initial phasing of all targets and observers. Notably, at every instant in time, all the targets possess an apparent magnitude that is visible to at least one observer. In addition to that, considering the effects of solar, Earth, and lunar exclusion, the target in the L_1 halo orbit is visible to the constellation of observers for 97.6% of the time, while the L_2 halo target is visible for 96.2% of the time. Intuitively, for targets in these two orbits, proximity to the Moon causes lunar exclusion effects that limit their visibility. The target in the DRO is visible for 99.7% of the propagation time, where a 5 hr period of exclusion due to the Earth limits visibility. However, this instance coincides with the perilune passage of the target in its orbit; as such, Earth-based observers may be utilized to supplement the observations of the constellation and retain custody of the target. Finally, the targets in the L_4

and L_5 SPOs are visible to the constellation of observers for the entirety of the propagation time. Thus, these observers are well-suited for surveillance of the region about the equilateral libration points. Additionally, the high spatial component of the observer orbits in this constellation, along with the synodic phasing, allow for these favorable viewing conditions to persist over subsequent revolutions.

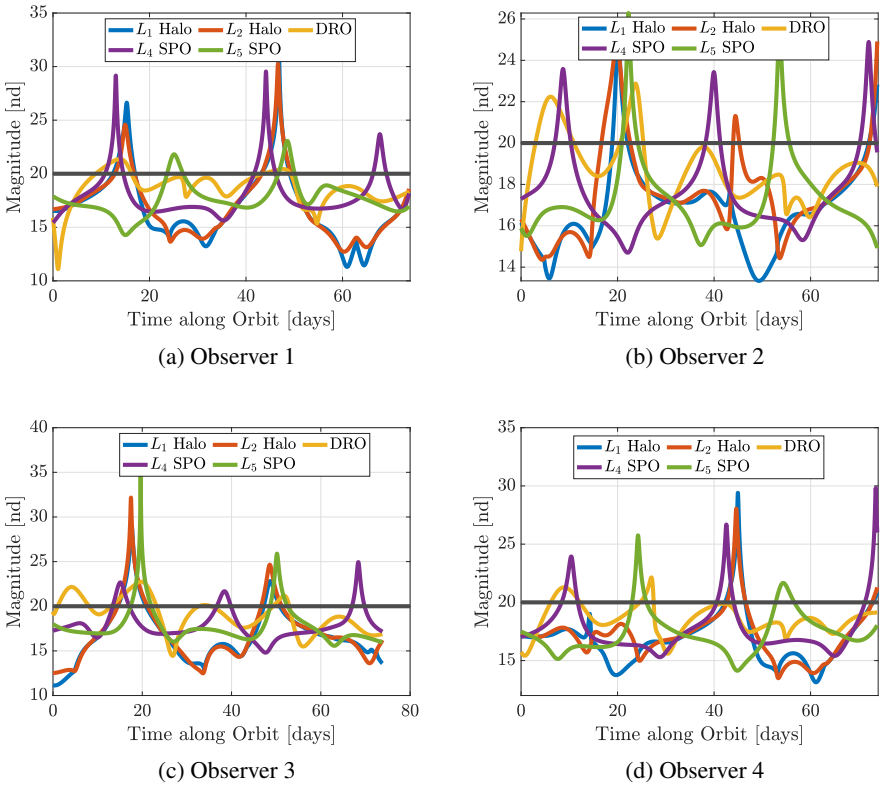

(a) Observer 1

(b) Observer 2

(c) Observer 3

(d) Observer 4

Figure 12. Apparent magnitude of the various targets in different orbits as viewed by each observer in the constellation at the initial relative phasing; then each evolving along the orbit.

CONCLUSIONS

The current work investigates the design and assessment of space-based optical observer trajectories to support cislunar operations beyond the GEO belt. The analyses presented in this work are accomplished in the Earth-Moon CR3BP, incorporating the gravitational influences of the Earth and the Moon on the observer trajectories. From certain sidereal resonant orbit families, specific orbits are identified that, in addition to being nearly sidereal resonant with the Moon, exhibit commensurability with the lunar synodic period as well. This characteristic arises due to the orbits being *nearly* sidereal resonant, that allows the family of sidereal resonant orbits to span a wide range of orbital periods in the rotating frame. Thus, the orbits retain the favorable geometries and stability properties inherent to their sidereal resonant structure, with the added advantage of repeatability with respect to the orientation of the Sun in the Earth-Moon rotating frame. These characteristics are leveraged to design observer trajectories in support of SSA operations beyond the vicinity of the Earth, where illumination and visibility conditions are evaluated.

Metrics for assessing the utility of cislunar trajectories for visibility and connectivity in this regime are introduced. Visibility criteria that are introduced include the observed target magnitude, and visibility relative to solar, Earth, and lunar exclusion zones. The fidelity of lunar exclusion zone modeling is improved by introducing the modified lunar exclusion zone that incorporates the lunar phase as seen by the observer. Fixed target locations near the Moon, as well as targets dispersed across the cislunar volume, are introduced and evaluated as viewed from candidate observer orbits. Additionally, leveraging known periodic solutions in the Earth-Moon CR3BP, targets operating in cislunar orbits are assessed for their visibility from space-based optical observers.

Orbits exhibiting the sidereal-synodic overlap allow the design of observer constellations that can overcome gaps in coverage by simultaneously sweeping through the cislunar domain. The sample scenario in the current work demonstrates total coverage of the cislunar domain in the presence of limiting magnitude and exclusion constraints. The synodic resonance of the observer orbits allows flexibility in trajectory design, since successful configurations repeat periodically. The current work employs representative values for the assessment of visibility conditions; the trajectory design and analysis framework is adaptable to incorporate other values as necessary.

ACKNOWLEDGEMENTS

The authors gratefully acknowledge support for this research from the Air Force Office of Scientific Research (AFOSR), in particular Dr. Stacie Williams, as part of the Space University Research Initiative (SURI), grant FA95502210092. The authors also appreciate valuable discussions with Prof. Carolin Frueh, Surabhi Bhadauria, and Noah Sadaka. Feedback from members of the Multi-Body Dynamics Research Group at Purdue University is also acknowledged.

REFERENCES

[1] "Memorandum of Understanding between the National Aeronautics and Space Administration and the United States Space Force," 09 2020. https://www.nasa.gov/wp-content/uploads/2015/01/nasa_ussf_mou_21_sep_20.pdf?emrc=a97009, last accessed at 2024-03-26.

[2] "Space Doctrine Publication 3-100, Space Domain Awareness," 11 2023. Space Training and Readiness Command (STARCOM), United States Space Force.

[3] M. Gupta, *Navigating Chaos: Resonant Orbits for Sustaining Cislunar Operations*. Ph.D. Dissertation, Purdue University, West Lafayette, Indiana, 2024.

[4] J. Williams, D. Lee, R. Whitley, K. Bokelmann, D. Davis, and C. Berry, "Targeting Cislunar Near Rectilinear Halo Orbits for Human Space Exploration," *27th AAS/AIAA Space Flight Mechanics Meeting*, San Antonio, Texas, 02 2017.

[5] M. Vaquero and K. C. Howell, "Design of Transfer Trajectories between Resonant Orbits in the Earth-Moon Restricted Problem," *Acta Astronautica*, 2014, 10.1016/j.actaastro.2013.05.006.

[6] E. M. Zimovan Spreen, *Trajectory Design and Targeting for Applications to the Exploration Program in Cislunar Space*. Ph.D. Dissertation, Purdue University, West Lafayette, Indiana, 2021.

[7] S. Bhadauria, C. Frueh, and K. C. Howell, "Cislunar Space Domain Awareness Using Bi-Circular Four Body Geometry," *AAS/AIAA Astrodynamics Specialist Conference*, Charlotte, North Carolina, 08 2022.

[8] M. Gupta and K. C. Howell, "Cislunar Eclipse Mitigation Strategies for Resonant Periodic Orbits," *AAS/AIAA Astrodynamics Specialist Conference*, Big Sky, Montana, 08 2023.

[9] M. Thompson, N. Ré, C. Meek, and B. Cheetham, "Cislunar Orbit Determination and Tracking via Simulated Space-Based Measurements," *Advanced Maui Optical and Space Surveillance Technologies Conference*, 09 2021.

[10] M. Holzinger, C. Chow, and P. Garretson, "A Primer on Cislunar Space," 06 2021. AFRL Space Vehicles Directorate, AFRL 2021-1271.

[11] C. Frueh, K. Howell, K. J. DeMars, and S. Bhadauria, "Cislunar Space Situational Awareness," *31st AAS/AIAA Space Flight Mechanics Meeting*, Charlotte, North Carolina (Virtual), 02 2021.

[12] D. A. Vallado, P. J. Cefola, R. Kiziah, and M. Ackermann, "Removing the Solar Exclusion with High Altitude Satellites," *AIAA/AAS Astrodynamics Specialist Conference*, 2016, 10.2514/6.2016-5433.

[13] "SPICE Data (SPICE Kernels)," 03 2024. https://naif.jpl.nasa.gov/naif/data.html, last accessed at 2024-03-10.

[14] C. Frueh, K. Howell, K. J. DeMars, S. Bhadauria, and M. Gupta, "Cislunar Space Traffic Management: Surveillance through Earth-Moon Resonance Orbits," *8th European Conference on Space Debris*, Virtual, 04 2021.

[15] J. L. Worthy III, M. Holzinger, and K. Fujimoto, "Optical sensor constraints on space object detection and admissible regions," *Advances in the Astronautical Sciences*, Vol. 150, 2014, pp. 93–112.

[16] J. K. Vendl and M. J. Holzinger, "Cislunar Periodic Orbit Analysis for Persistent Space Object Detection Capability," *Journal of Spacecraft and Rockets*, 2021, 10.2514/1.A34909.

[17] E. E. Fowler and D. A. Paley, "Observability Metrics for Space-Based Cislunar Domain Awareness," *Journal of the Astronautical Sciences*, Vol. 70, 04 2023, p. 10, 10.1007/s40295-023-00368-w.

[18] N. Kinzly, B. Polzine, C. Short, and J. Woodburn, "Simulating a Dynamics-Informed Cislunar RPO Mission Incorporating Orbit Determination," *AAS/AIAA Astrodynamics Specialist Conference*, Charlotte, North Carolina, 08 2022.

[19] D. Somavarapu, D. Guzzetti, and S. Hesar, "Feasibility Studies for an Autonomous Cislunar Position, Navigation and Timing Constellation," *AAS/AIAA Astrodynamics Specialist Conference*, Charlotte, North Carolina, 08 2022.

[20] J. J. Roth and E. J. Felt, "Overcoming Technical Challenges from Low Earth Orbit to Cislunar," *Advanced Maui Optical and Space Surveillance Technologies (AMOS) Conference*, Maui, Hawaii (Virtual), 09 2020.